Volume 18
Number 48
28 December 2022
Pages 9125–9300

Soft Matter

rsc.li/soft-matter-journal

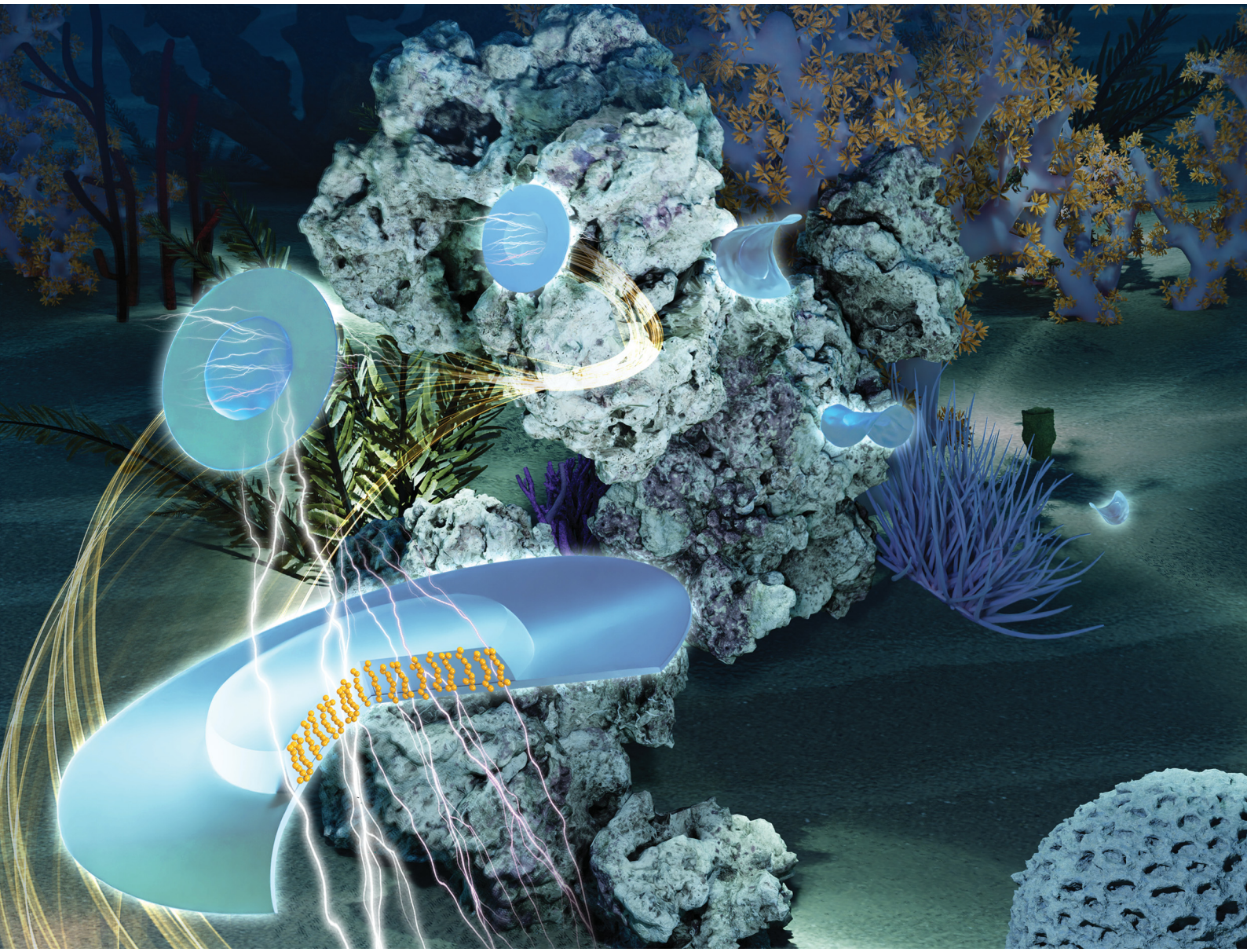

ISSN 1744-6848

ROYAL SOCIETY OF CHEMISTRY

PAPER
Huichan Zhao *et al.*
Stretchable and conformable variable stiffness device through an electrorheological fluid

Soft Matter

PAPER

View Article Online
View Journal | View Issue

Cite this: *Soft Matter*, 2022, **18**, 9163

Stretchable and conformable variable stiffness device through an electrorheological fluid†

Yiyi Pan,[abc] Xin-Jun Liu[abc] and Huichan Zhao*[abc]

Stiffness variations extend creatures' functions and capabilities to deal with complex environments. In this study, we proposed an electrorheological fluid-based variable stiffness device, named VSERF, made up of soft materials. Our device is soft, thin, and stretchable so that it can conform to surfaces with complex morphologies. The stiffness of the VSERF device can be continuously, independently, and reversibly adjusted by applying an electric field. It achieves 14.8-times compressive stiffness variation and 3.5-times tangential stiffness variation when the electric field intensity increases from 0 V mm^{-1} to 750 V mm^{-1}. The VSERF device is able to return to its initial shape after removing the external force and electric field, allowing it to be reused. The effects of stretching and bending on the device's capability of stiffness variations are investigated experimentally and the results show that the stiffness variation is unaffected by a stretching strain of up to 20% and a bending curvature of up to 50 m^{-1}. Finally, we show that the VSERF device is capable of conforming to complex surfaces (coral stones, pencils, and 3D printed cubes) in its inactive state, hanging on them with a weight of up to 80 g (19 times of its own weight) in its active state, and detaching when the electric field is removed. The device's short-term and long-term stabilities are experimentally investigated as well. The demonstration of the VSERF's attaching and detaching ability shows that the stiffness-variation device's adaptability to complex environments can be improved.

Received 13th October 2022,
Accepted 30th October 2022

DOI: 10.1039/d2sm01362b

rsc.li/soft-matter-journal

1 Introduction

In nature, creatures actively adjust the stiffness of their tissues to meet various functional requirements in complex environments. For example, sea cucumbers harden their skins rapidly to protect their internal bodies when attacked by enemies;[1] fish adjust the stiffness of their tail fins to improve swimming efficiency;[2] flies adjust the stiffness of their pterygoid muscles in real time to control the dynamic motions of their wings;[3] elephant trunks and octopus' limbs[4] can switch their stiffness to achieve multiple functions.

From bioinspiration and biomimetics, stiffness variation is introduced to mechanical systems to improve their performance and extend their functionalities.[5–9] Several stiffness variation methods were developed, such as the antagonistic stiffness-variation method, jamming-based method, phase-change-based stiffness variation method, *etc.*[10] The antagonistic methods regulate stiffness by driving actuators (*e.g.*, McKibben artificial muscles) simultaneously that are arranged antagonistically.[11] The jamming-based methods increase stiffness by adjusting the internal forces of friction between particles while being vacuumed.[12] Smart materials include temperature-driven materials,[13–15] magnetically driven materials,[16] and electrically driven materials that can also regulate their stiffness through phase changes.[17] Based on the above methods, a series of variable stiffness devices have been developed, such as grippers,[18] mobile robots,[19] wearable devices,[20] artificial skins,[21] surgical manipulators,[22] *etc.* However, the practical applications of variable stiffness devices are hindered by their bulky and heavy body, small stiffness-variation range, slow response speed, irrecoverable deformation, and non-continuous stiffness change.[23]

Electrorheological fluid (ERF) is a type of smart material whose rheological properties can change reversibly under an electric field. ERF is mainly composed of a liquid phase and a particle phase. The liquid phase is usually insulated, and the particle phase usually has a high dielectric coefficient. On the micro-scale, the particles in an ERF change from a disordered state to chains or columnar structures along the direction of the electric field due to the attractive forces between polarized particles, which cause the continuous and fast transformation of the ERF from liquid state to quasi-solid on the macro-scale.[24,25] This changing process involves both the viscosity

[a] *Department of Mechanical Engineering, Tsinghua University, Beijing 100084, China*
[b] *State Key Laboratory of Tribology in Advanced Equipment, Beijing 100084, China*
[c] *Beijing Key Lab of Precision/Ultra-Precision Manufacturing Equipment and Control, Beijing 100084, China. E-mail: zhaohuichan@mail.tsinghua.edu.cn; Tel: +86(010)62780957*

† Electronic supplementary information (ESI) available: Movies S1 and S2. See DOI: https://doi.org/10.1039/d2sm01362b

variation and the stiffness variation of the ERF. Most of the reported studies investigated the viscosity change of ERFs and the characteristic of damping variation was used to develop a variety of dampers,[26–28] clutches,[29,30] tactile sensors,[31,32] and valves.[33–35]

A few other scholars have studied the stiffness-variation characteristics of an ERF. Wang *et al.* proposed a boring system that can increase its rigidity with an increase in the electric field by encapsulating an ERF in its boring bar, which increases the stability during boring and improves the machining quality.[36] Yuan *et al.* attached an ERF-based stiffness-variation structure on a soft pneumatic bending actuator to suppress the actuator's intense vibration during operation. Results showed that the vibrational amplitude and decay time of the bending actuator upon step input were reduced by 62.3% and 48.3%, respectively, when an electric field of 3 kV mm^{-1} was applied across the ERF.[37] Behbahani *et al.* proposed a stiffness-variation ERF-based cantilever beam, whose natural frequency could increase by up to 40% with an applied electric field.[38] The abovementioned studies have achieved stiffness-variations effectively using an ERF, yet the stiffness-variation ratio (defined as the enhanced stiffness with an electric field divided by its original stiffness) is still low (less than 10), especially when compared with ERF's own remarkable capability of changing its viscoelastic characteristics (the complex modulus of an ERF can change by several orders of magnitudes). One of the reasons is that the materials for encapsulating and the electrodes for powering an ERF were rigid. These rigid materials increased the baseline stiffness of the composite structure with an ERF, limiting its stiffness-variation-ratios as a result.

In this study, we propose a stiffness-variation device based on an electrorheological fluid, named VSERF, which is lightweight, thin, soft, and stretchable, with a stiffness-variation ratio of greater than 10. We achieve this relatively larger stiffness-variation ratio by selecting soft materials for encapsulating the ERF and soft electrode materials for powering the ERF. These soft materials maintain the high compliance of the device with no electric field being applied; thus, the VSERF device can be conformed to a variety of complex surfaces. We also demonstrated that the VSERF device can be stretched up to a 20% strain, bent up to a 50 m^{-1} curvature, and used repeatedly. Finally, we demonstrated the functionality of our proposed device by an ''attaching and detaching'' experiment to different surfaces and investigated its short-term and long-term stabilities.

2 Materials and methods

2.1 Device design

Structural design of the VSERF device. To facilitate the application of an electric field, the devices based on ERFs are usually fabricated in a sandwich configuration, which is also adopted in our study. Two stretchable electrodes are symmetrically distributed on the very top and bottom outer sides and the ERF is sandwiched in between. Due to its liquid characteristics, the ERF needs to be encapsulated to maintain a definite shape and thus we designed a packaging layer made of elastomers between the ERF and each electrode. Therefore, the device, named VSERF, eventually exhibits a five-layer liquid-elastomer-composite structure as shown in Fig. 1a. The whole device maintains a state of stretchability and softness as a result of our selected materials. It can be bent, stretched, and pressed as shown in Fig. 1b.

Selection of materials. Selecting soft and stretchable materials to construct a thin, soft, stretchable, and reliable stiffness-variation device is an important goal of this study, as we mentioned earlier. Due to the amorphous state of the ERF (Ningbo Maiwei Technology, Co., LTD), there must be a solid material for encapsulating the ERF so as to construct a definite shape device. Besides the above requirement, we also require the encapsulating material to have low permeability and low swelling tendency in the ERF's liquid phase. Silicone rubbers, hydrogels, and polyurethane rubbers were all taken into consideration initially; however, the severe swelling between the silicone rubber and the ERF's liquid phase (which is silicone oil), and the water loss from hydrogels over time would dramatically accelerate the sedimentation of the ERF. Therefore, in this study, a low-modulus polyurethane rubber (VytaFlex™ 10 from Smooth-On, Inc.) was selected as the encapsulating material due to its inertness to the ERF both chemically and physically. For electrodes, thin layers of networked carbon nanotubes (CNTs, from Nanjing XFNANO Co., LTD) were selected due to their high stretchability and satisfactory conductivity.[39] Sealing materials are used to bind the upper and lower encapsulating layers and form an airtight shell and we chose polyurethane-based adhesives (URE-BOND™ II from Smooth-On, Inc.). A bonding material is used to bind the power wires to the electrodes, and it needs to have strong adhesion and high conductivity. In this study, silver epoxy resin (8331 silver conductive epoxy adhesive from MG Chemicals) was chosen as the bonding material to enable an efficient and reliable power transmission between the power supply and the device.

The working principle of the device. The device's two electrodes are connected to a high-voltage power supply through wires so that an electric field can be applied between the electrodes and the ERF. Driven by the electric field, the particles in the ERF are assembled into chains or columnar structures along the direction of the electric field, which enhances the ERF's ability to resist deformation, thus showing the effect of stiffness enhancement. Once the electric field is removed, the mutual attractions between particles are weakened, thus weakening the ability of the ERF to resist deformation, and showing the effect of stiffness reduction. At the same time, because the ERF's ability to resist deformation is related to the strength of the chains or columnar structures assembled by particles, and the strength is related to the electric field intensity, the stiffness of the device can be adjusted by adjusting the electric field intensity continuously.

2.2 Manufacturing of the VSERF device

The manufacturing process of VSERF is shown in Fig. 1c. The process consists of three major steps: the manufacturing of the

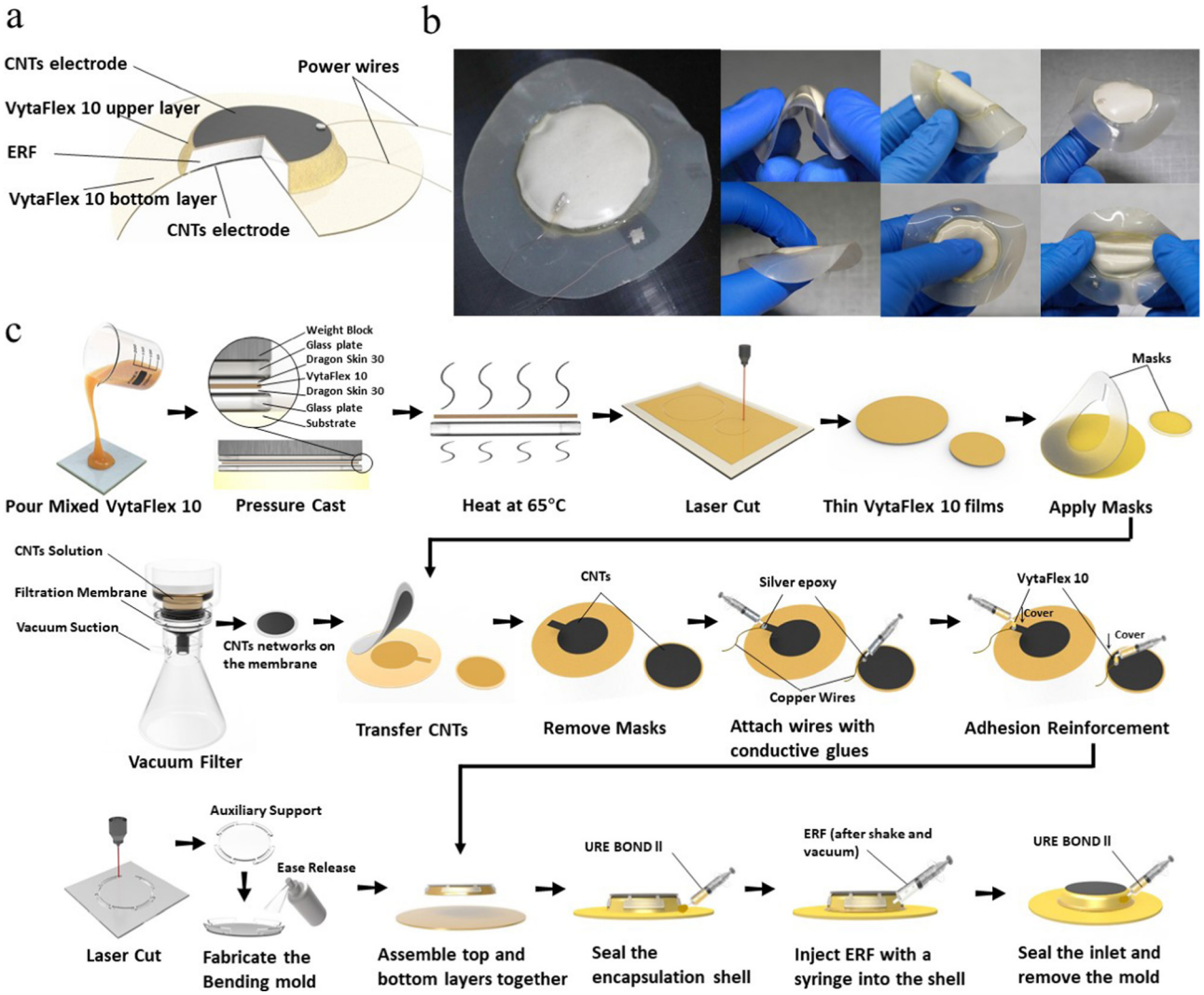

Fig. 1 Design and manufacturing of the VSERF device. (a) Sandwiched configuration of the VSERF device with the CNT electrodes distributed in the very outer layers of the device and the ERF encapsulated in the chamber formed by two layers of VytaFlex 10 films. (b) Photographs show the characteristics of thin, soft, and stretchable VSERF, which will enable this device to be integrated with various systems. (c) Manufacturing processes of the VSERF.

encapsulating layers (the first row in Fig. 1c), the fabrication and application of CNT electrodes (the second row in Fig. 1c), and the sealing and injection procedures (the third row in Fig. 1c).

Manufacturing of the encapsulating layers. Thin films made of VytaFlex 10 were cast following three stages: pre-elastomer mixing, casting in a designed mold, and curing. In the molding stage, the bonding strength and wettability between VytaFlex 10 and the mold's internal surface played critical roles in the successful casting and release of the cast film. Excessive bonding strength leads to difficulty in demolding whereas insufficient wettability causes the agglomeration of the pre-elastomers during casting. To overcome these challenges and obtain a uniform, thin polyurethane film, we first spin-coated a thin film of a silicone elastomer (Dragon Skin™ 30 from Smooth-On, Inc.) on the mold (specifically, two pieces of flat and smooth glasses formed the mold), and then we poured the polyurethane pre-elastomer onto it to avoid the excessive bonding between the cured polyurethane rubber and the glass. To avoid agglomeration during casting, we applied pressure on the mold with a weight block during the curing procedure. As a result, the small bonding force between polyurethane and silicone enabled the easy release of the cured film, and the applied pressure guaranteed the uniformity of the film. The thickness of the film could be controlled by adjusting the weight of the block. After these steps, the material was left at room temperature for 24 hours and then baked in an oven for 4 hours for complete curing. Finally, thin films with a uniform thickness of up to 200 microns were obtained through the above stages. Laser cutting was used to get the designed shape and dimension of the top and bottom encapsulating films (see schematics in the first row of Fig. 1c).

Fabrication and application of CNT electrodes. The vacuum filtration method was used to fabricate thin films of networked CNTs. A filtration membrane was placed between the CNT solution and a fine mesh fixed on a conical flask's neck. The

solvent in the CNT solution flowed into the conical flask through the mesh and the filtration membrane during vacuuming, whereas the solute was left uniformly distributed on the filtration membrane, forming a film of networked CNTs. The thickness of the film was determined from the weight percentage of CNTs in the solution. The CNT film on the filtration membrane was then transferred onto the encapsulating film through a mask. Copper wires were bonded onto the CNTs through silver epoxy adhesives. However, the solidified silver epoxy did not form a firm connection with the film made of VytaFlex 10; therefore, URE-BOND™ II was used to reinforce the connection (see schematics in the second row of Fig. 1c).

Sealing and injection. To construct a three-dimensional enclosed shell to house the ERF, an auxiliary bending mold was made by laser cutting to shape the top encapsulating film into a pan shape. A release agent (Ease Release™ 200 from Smooth-On, Inc.) was sprayed onto the mold to enable its removal. The top and bottom encapsulating layers were assembled and sealed with URE-BOND™ II, forming a 3D enclosed shell as shown in the third row in Fig. 1c. Then we shook and vacuumed the ERF to ensure its uniform concentration and removal of air left in the content. A syringe was used to inject a certain volume of the ERF into the enclosed shell to obtain a thickness of 3.5 mm for the VSERF device. Finally, the injection inlet was sealed and the bending mold was removed. In our design, the diameter of the closed shell was 30 mm (without the edge), and the diameter of the whole device (with the edge) was 60 mm. The total weight of the device was about 4 g. To ensure safety, we chose a power supply (TCM6000, Dalian Teslaman Tech. Co., Ltd) with the function of overcurrent protection.

2.3 Characterization of the ERF

The stiffness variation capability of the VSERF device is mainly determined using the encapsulated ERF material. The ERF presents a half-solid–half-liquid state with the application of an electric field and thus can be regarded as a viscoelastic material.[40] The amplitude sweep method was adopted to measure the storage modulus of the ERF at different driving electric field intensities using a rheometer (MCR 302 from Anton Paar Inc.). A schematic diagram of the experiment setup is shown in Fig. 2a. The ERF was loaded into the cylindrical stator of the rheometer. The rotor was immersed into the ERF and a fixed space of 1 mm between the rotor and the stator was formed. The stator was connected to the negative pole of the power supply and the rotor was connected to the positive pole, so that a uniform electric field was applied between the stator and the rotor, across the ERF material. The rotor was subjected

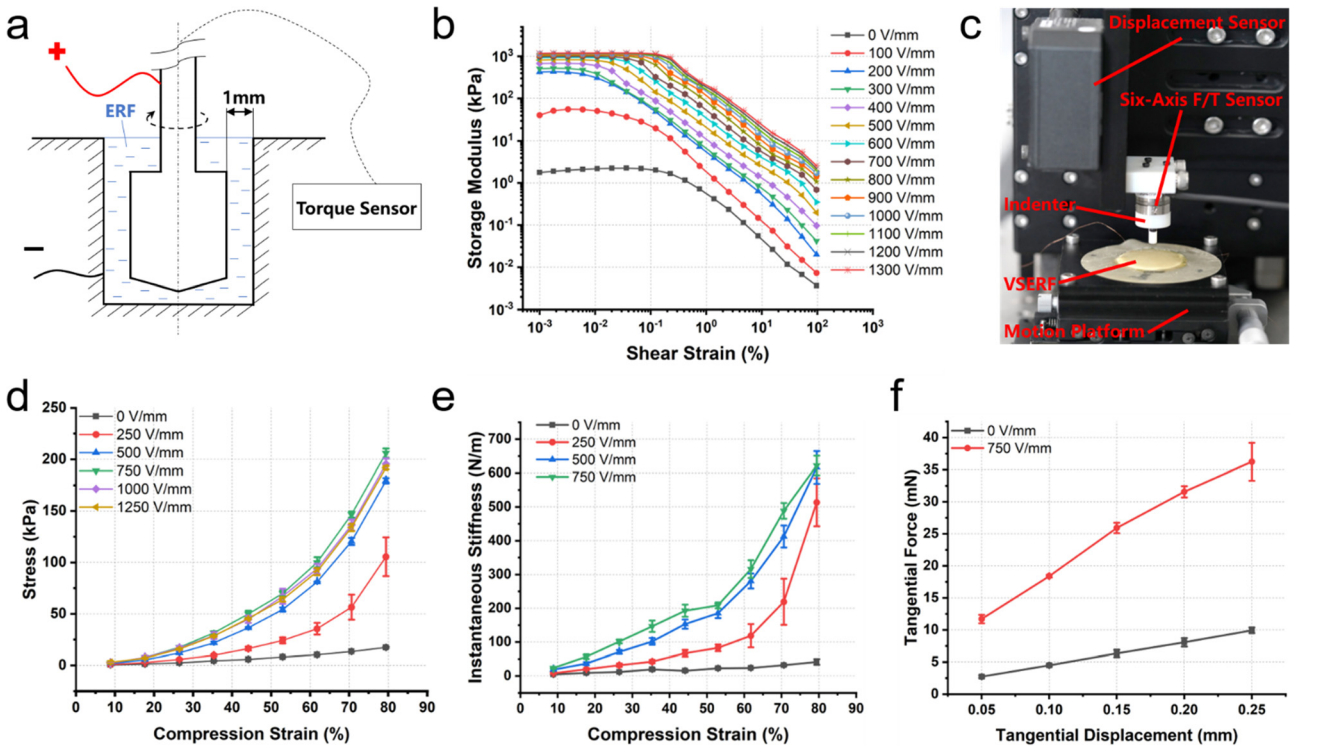

Fig. 2 Characterization of the stiffness-variation range of the ERF material and the VSERF device. (a) Schematic diagram of the experimental setup for ERF's rheological measurement. (b) Storage modulus of ERF at different electric field intensities. (c) Photograph of the experimental setup for stiffness measurement of the VSERF. (d) Compressive stress–strain relationship of VSERF at different electric field intensities. The error bars indicate the standard deviations of the measured stress with tests being repeated three times. (e) Calculated instantaneous stiffness of the VSERF along the compression direction at different electric field intensities. The error bars indicate the calculated standard deviations of the instantaneous stiffness. (f) Tangential stiffness at different electric field intensities of the VSERF device. The error bars indicate the standard deviations of the measured force, with tests being repeated three times.

to a preset oscillating shear strain (the frequency was fixed at 1 Hz), and its stress caused by the viscoelastic resistance of the ERF was measured using the torque sensor attached to it. The storage moduli of the ERF at various shear strains at different electric field intensities from 0 V mm^{-1} to 1300 V mm^{-1} were measured, as shown in Fig. 2b. For any curve of storage modulus at a fixed intensity of the electric field, it can be observed that the storage modulus of the ERF remains at a constant value, the so-called plateau value, in the linear viscoelastic (LVE) regime. The storage modulus decreased significantly when the shear strain was beyond the limit of the LVE range which indicates the ERF yields and is no longer seen as purely elastic. The limit of the LVE range is defined as the first point which deviates from the initial plateau value up to 10%.[41] The storage modulus of the ERF increases with the electric field intensity as well, indicating an increased stiffness. The increasing trend, however, gradually declined. It is worth noting that at least two orders of magnitude of stiffness variation ($\sim$500 times) were achieved when the electric field intensity was increased from 0 V mm^{-1} to 1300 V mm^{-1}. This is a remarkable range of stiffness variation compared with those of ER elastomers[42] and stiffness-variation devices based on ERFs,[36–38] indicating its great potential for developing devices with more effective stiffness variation.

3 Results and discussion

3.1 Characterization of VSERF's stiffness-variation capability

Characterization of the stiffness-variation range of the VSERF device. The stiffness of the proposed VSERF device can be defined in different directions. In our study, we focus on its axial compressive stiffness and tangential stiffness. The experimental setup to measure stiffness is shown in Fig. 2c, in which an indenter was connected with a six-axis force/torque (F/T) sensor, and it was controlled gradually to press into the VSERF device along the thickness direction to characterize its axial compressive stiffness, or to slide horizontally along the plane direction to characterize the tangential stiffness. During the pressing process, the force collected by the force/torque sensor was F, the area of the indenter was S_0, the thickness of the device was t_0, and the compressive displacement of the indenter was x. The compression strain ε was calculated as follows:

$$\varepsilon = x/t_0 \quad (1)$$

The compression stress σ was calculated as follows:

$$\sigma = F/S_0 \quad (2)$$

The compression strain–stress relationship was plotted as shown in Fig. 2d, from which we clearly observe that the stiffness of the VSERF device (defined as the slope of the curves) generally increases with the applied electric field intensity and reaches its maximum when the applied electric field intensity reaches 750 V mm^{-1}. To better exhibit the non-linearity of stiffness with strain, instantaneous stiffness k_{ins} was defined as follows:

$$k_{ins} = \Delta F/\Delta x \quad (3)$$

We have plotted k_{ins} with strain as shown in Fig. 2e and it can be observed that the instantaneous stiffness of the VSERF increases with the compressive strain.

When the applied electric field intensity increased from 0 V mm^{-1} to 750 V mm^{-1}, it can be calculated that the instantaneous stiffness of VSERF increased by 6–14.8 times depending on the compression strain. Specifically, at a compression strain of 80%, the instantaneous stiffness of the device increased from 42 N m^{-1} to 622 N m^{-1} (14.8 times). Then we characterized the device's tangential stiffness variation. The procedure was as follows: the indenter was pressed in the device to prevent slippage between the indenter and the surface of the device, and a controlled tangential displacement was given to the indenter while the tangential force was collected using a six-axis F/T sensor installed on the indenter. The result (Fig. 2f) shows that when the applied electric field intensity was increased from 0 V mm^{-1} to 750 V mm^{-1}, the tangential stiffness of VSERF (defined by the slope of the displacement–force curves) increased from 40 mN mm^{-1} to 145 mN mm^{-1} (3.5 times). To summarize, we have experimentally found the optimal operating electric field intensity to be 750 V mm^{-1}, and the stiffness variation range was up to 14.8 times. Besides, the stiffness variation of the VSERF device occurred not only in its thickness direction but also in its plane direction. However, the stiffness variation was anisotropic because the maximum tangential stiffness variation range was only 3.5 times.

Characterization of VSERF's shape recovery capability. For the device to be used repeatedly and continuously, it is necessary for the device to possess the capability of recovering from a deformed shape to its original shape when external forces are removed (this is what we call as ''elastic'', rather than ''viscous''). Several stiffness-variation strategies require extra steps to recover to the initial shape after stiffness variation, such as a massage (repeated press, rub, and pinch).[43] Poor shape recovery ability of the device causes difficulty in practical uses in continuous tasks. In this study, the elastic films as the encapsulating layer not only enclose the ERF to form a solid-state device but also provide the elastic force to recover to the device's initial shape. To enhance such elastic forces, the films should be set at a pre-tensioned state by filling excessive ERFs. When the ERF is in its low-modulus state with no electric field applied, the device could recover to its original shape through the elastic force stored in the elastic film when the external force is removed. When the ERF is in a high-modulus state with the applied electric field, the device has a function of shape locking and its characteristic is more like a damping, so it does not recover after the external force is removed. After removing the electric field, the device will gradually restore its original shape under the elastic force of the elastic film. To characterize this shape recovery ability of the device, the following experimental steps were implemented (illustrated in Fig. 3a): in the soft state of the device, a compression strain was applied by the indenter, an electric field was applied to the device to lock the shape, the indenter was removed, and then the electric field

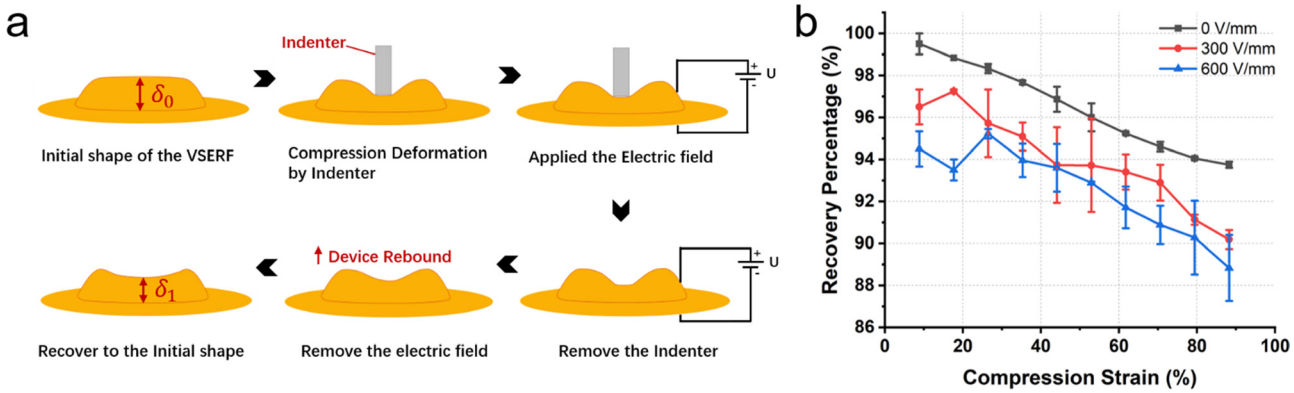

Fig. 3 Characterization of the VSERF's shape recovery capability. (a) Illustration of the shape recovery behaviour of VSERF. (b) Recovery percentage of VSERF under different compression strains and at different electric field intensities. The error bars indicate the standard deviation of the calculated recovery percentage from three measured times.

was removed. The recovery displacement of the device was recorded two minutes after the electric field was removed. We repeated this process and recorded the recovery displacement at each compression strain at different electric field intensities. The recovery percentage η was calculated as the recovered thickness δ_1 over the original thickness δ_0 as follows:

$$\eta = \delta_1/\delta_0 \quad (4)$$

Even if the shape recovery percentage of the device decreased as we increased the compression strain and the applied electric field, over 85% of recovery could still be achieved (Fig. 3b). The device's shape recovery ability was affected by the electric field intensity, which may be due to the residual stress present in the particle chains formed in the ERF under the electric field, hindering the restoration force from the elastic film. In specific applications, gravity can also be utilized to further assist the device to recover to its initial shape.

The effect of stretching on the VSERF's stiffness variation. Stretchability is an important characteristic of an attachable device as it enables the device to conform to stretchable surfaces, such as the stretching segments of soft actuators. Therefore, the influence of stretching on the VSERF's stiffness variation is necessary to be investigated. In this experiment, the device was stretched to different strains as shown in Fig. 4a. The compressive stress–strain relationship of the VSERF under 750 V mm^{-1} after stretching to different strains (from 0% to 100%) was measured (the experimental setup was the same as shown in Fig. 2c). The results are shown in Fig. 4b.

The results show that when the stretching strain was smaller than 20%, the stiffness (slope of the stress–strain curve) of the device was almost unaffected. When the strain got larger than 20%, the stiffness variation range dropped with strain. When the device was stretched to a strain of 100%, its stiffness decreased to only 30% of its achievable stiffness at 750 V mm^{-1} with no stretching and thus the stiffness variation ratio decreased from 20 times to only 4 times (Fig. 4c). The decrease in stiffness could be partially explained by the failure of networked CNTs under large strains.

The effect of the attached surface's curvature on the VSERF's stiffness variation. The soft, thin, and stretchable characteristics of the proposed device enabled its excellent conformability to complex shapes other than flat surfaces. In practical applications, the device needs to be attached to surfaces with different curvatures. Therefore, it is important to study the influence of

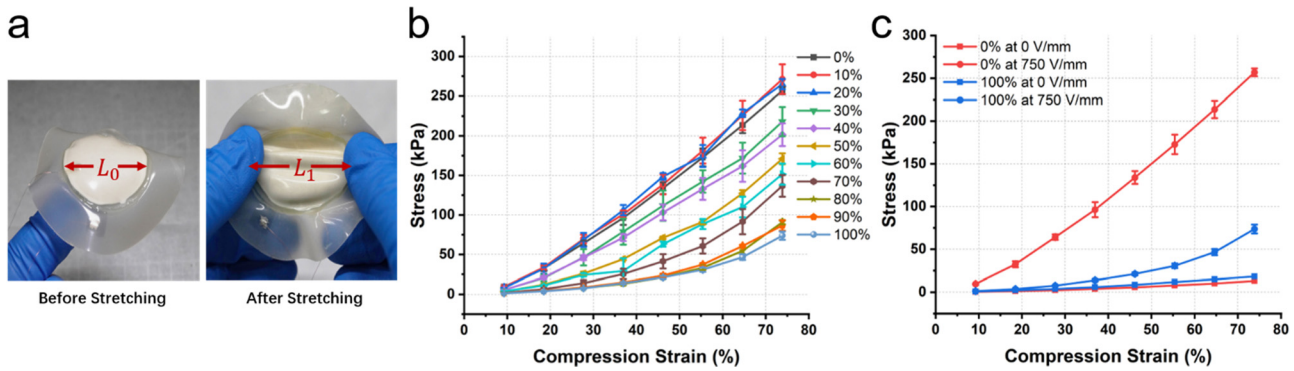

Fig. 4 Characterization of the effect of stretchability on VSERF's stiffness variation. (a) Photographs of the device before and after stretching. (b) Compression stress–strain relationship of the VSERF after stretching to different tensile strains under a 750 V mm^{-1} electric field. The error bars indicate the standard deviations of the measured stress from three times repeated experiments. (c) Stiffness variation of the device under 0 V mm^{-1} and 750 V mm^{-1} under 0% and 100% strains. The error bars indicate the standard deviations of measured stress from three times repeated experiments.

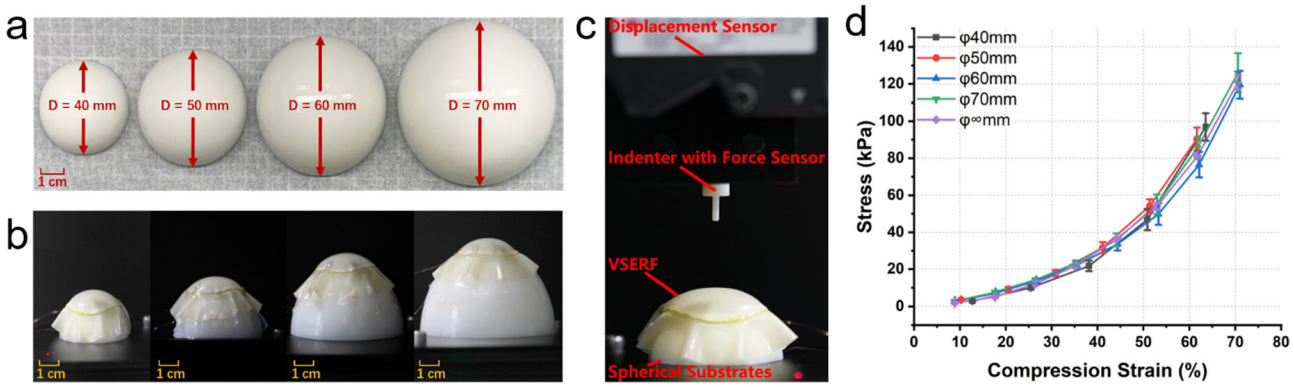

Fig. 5 Characterization of the conformability of the VSERF. (a) Spherical substrates with different curvatures (their diameters are 40, 50, 60, and 70 mm, respectively). (b) VSERF attaches to different surfaces of spherical substrates and conforms to different curvatures. (c) Experimental setup to measure VSERF's stiffness when attached to a spherical surface. (d) Compression stress–strain relationship of the VSERF when attached to a surface with different curvatures. The error bars indicate the standard deviations of the measured stress from three times repeated tests.

the attached surface's curvatures on the stiffness variation characteristics of the device. In this experiment, several spherical substrates with different curvatures were provided as the attached objects (shown in Fig. 5a, curvature up to 50 m^{-1}), and the compressive stress–strain relationship of the device attached to these surfaces with different curvatures was studied (setup shown in Fig. 5b and c). The result in Fig. 5d shows that the curvature of the attached surface has a negligible influence on the stiffness variation of the VSERF device, which demonstrates the satisfactory conformability of our proposed VSERF.

3.2 Demonstration of the VSERF's attaching and detaching ability

The purpose of designing a variable stiffness device is to integrate the soft and stiff characteristics simultaneously in a system so that the device can achieve more functions to meet

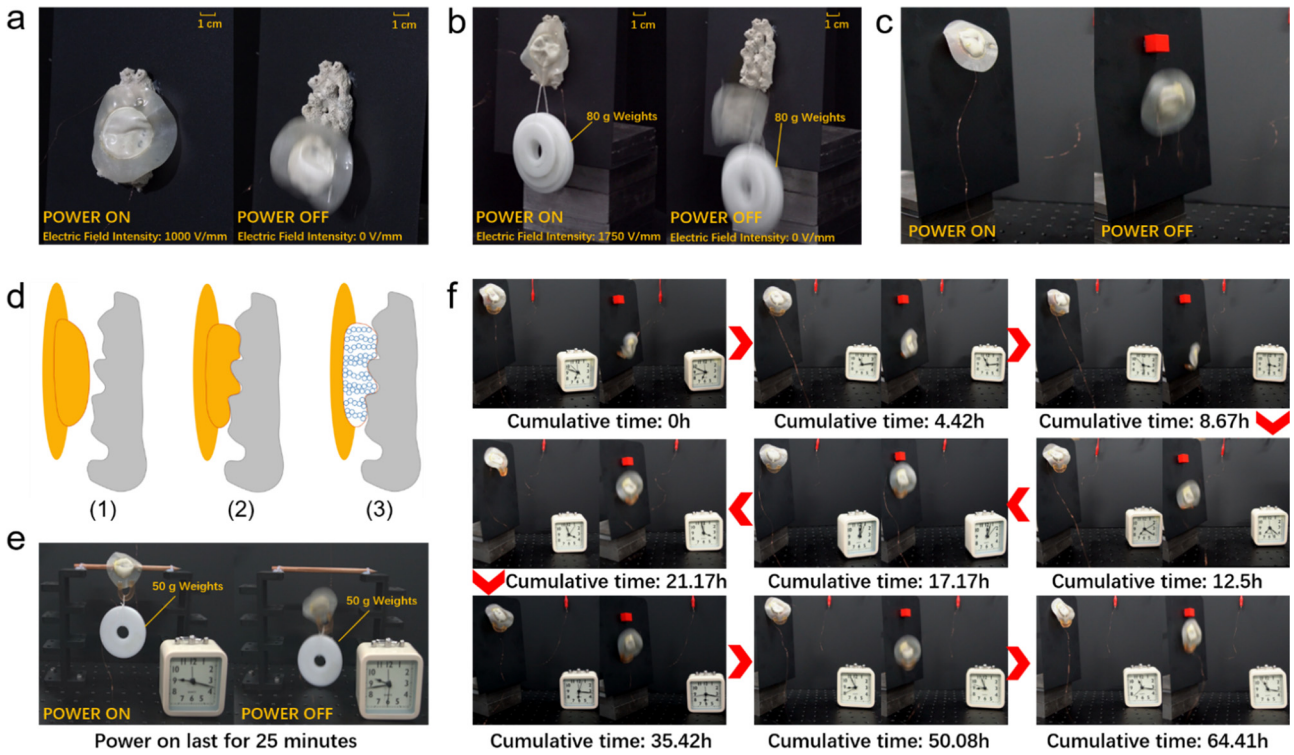

Fig. 6 Demonstration of the VSERF's attaching and detaching ability on different surfaces. (a) When an electric field is applied, the VSERF hangs on the coral stone and when the electric field is removed, the VSERF drops. (b) Attaching and detaching performance of the device with a load of 80 g, which is 19 times its own weight. (c) Demonstration of the VSERF's attaching and detaching process on a cube. (d) Diagrams showing the principle of attaching and hanging on surfaces of the VSERF. (e) VSERF with a 50 g weight hanging on a beam for 25 minutes with the electric field applied, which detached when the power was off. (f) Long-term tests of the device's reusability for attaching and detaching for 64.4 hours.

various needs. To verify the capability of the variable stiffness device, we have demonstrated the ability of the VSERF device to attach to complex surfaces and then detach. We fixed a coral stone on the wall, and then we attached the proposed VSERF to this rough surface in its soft state. The high compliance and thin morphology allow VSERF to conform to a variety of irregular surfaces. When an electric field was applied to the device, the high stiffness held it on the surface like sticking to it. We also hung weights on the VSERF when it was in its stiff state. The excellent force transmission performance of the device allows it to hold up to 80 g at 1750 V mm^{-1}, almost 19 times of its own weight. When the power was turned off, the VSERF could not hold its own gravity and dropped (Fig. 6a, b and Movie S1, ESI†). To demonstrate the VSERF's capability to attach to more geometries, especially those with sharp angles (which might lead to the damage of the device during attaching), we tested its attaching and hanging performance on a 3D-printed cube, as shown in Fig. 6c. The results show that it successfully attached and hung on the cube without any mechanical or electrical damage.

The important steps of the attaching and hanging process are illustrated in Fig. 6d. In step (1), with no electric field applied, the ERF is in its liquid form and the composite structure exhibits a soft and stretchable state. In step (2), when the VSERF is pressed onto a rough surface, it conforms to the surfaces due to its high compliance. In step (3), if the electric field is applied to the VSERF, the internal particles form linear or columnar granular chains and the ERF turns to a semi-solid state, being able to resist deformation upon forces. Therefore, it successfully holds its shape and hangs on irregular surfaces.

Besides the variety of attachable surfaces, the stability and reusability of the device are also important for its practical application. Sedimentation is a common process in the degradation of ERF-based devices.[42] There are several factors that can accelerate sedimentation, such as being in contact with the moisture in the air, the swelling tendency of some polymers such as silicone rubber with the silicone oil in ERF, *etc.* To better understand the time-stability and the reusability of our proposed VSERF, we have conducted two tests. The first experiment is to explore the one-time duration of the device to be hung on a surface or an object. The VSERF was attached to a pencil in the soft state and hung with a 50 g weight in the stiff state with the electric field applied for a relatively long duration of up to 25 minutes. Then we shut off the power, and the VSERF successfully detached from the pencil, which demonstrated that the device was still functional (Fig. 6e, and Movie S2, ESI†). The second experiment is to explore the long-term stability and reusability of the device. We tested the attaching and detaching capability of the device at regular intervals for about 2.5 days (64.4 hours). The device was demonstrated to be functional for at least 9 repeats for up to 64.4 hours (Fig. 6f), which preliminarily demonstrated the relatively long-term stability and reusability of our device. Currently, the lifetime of the device may be determined from the sedimentation effect of the ERF and the slow swelling and permeability effects between the ERF's liquid phase and encapsulating materials.

In these demonstrations, the device shows its ability to interact with unstructured surfaces in the soft state, and its ability to resist deformation applied by an external force in its stiff state. Furthermore, this demonstration shows the ability of the VSERF device to conform to and hold on rough surfaces due to its soft and stretchable characteristics. In the future, it could be further extended as a new perching mechanism for micro-aerial vehicles.

4 Conclusions

In this study, we proposed a thin, fully-soft, and stretchable ERF-based variable stiffness device (VSERF) with excellent conformability in its soft state and excellent load-bearing capability in its stiff state. The VSERF device is easy to integrate with other systems, including soft systems, and can be attached to a variety of surfaces to achieve stiffness variation. The VSERF's manufacturing process is scalable and has the potential to develop devices of a wide range of dimensions and shapes. Due to the advantages of the ERF, the stiffness of the VSERF device can be controlled independently, reversibly, repeatedly, and continuously and the response times of stiffening and destiffening are short. The above characteristics show that the device may have many practical applications in the future, such as developing a new perching mechanism, robotic skins, and multifunctional units.

Author contributions

Y. P. contributed to the data curation, investigation, methodology, formal analysis, and writing – original draft and X. L. contributed to the conceptualization, investigation, and writing – review and editing. H. Z. contributed to the conceptualization, investigation, methodology, supervision, and writing – review and editing.

Conflicts of interest

The authors applied for a patent (no. 202211016909.7) related to the work through Tsinghua University.

Acknowledgements

This work was supported by the National Natural Science Foundation of China under grant no. 52222502, 51975306, and 92048302.

Notes and references

1 J. R. Capadona, K. Shanmuganathan, D. J. Tyler, S. J. Rowan and C. Weder, *Science*, 2008, **319**, 1370–1374.
2 Q. Zhong, J. Zhu, F. E. Fish, S. J. Kerr, A. M. Downs, H. Bart-Smith and D. B. Quinn, *Sci. Rob.*, 2021, **6**, eabe4088.
3 M. H. Dickinson, C. T. Farley, R. J. Full, M. A. R. Koehl, R. Kram and S. Lehman, *Science*, 2000, **288**, 100–106.

4 G. Sumbre, G. Fiorito, T. Flash and B. Hochner, *Nature*, 2005, **433**, 595–596.
5 R. Baines, S. Freeman, F. Fish and R. Kramer-Bottiglio, *Bioinspiration Biomimetics*, 2020, **15**, 025002.
6 T. Sun, Y. Chen, T. Han, C. Jiao, B. Lian and Y. Song, *Robot. Comput. Integr. Manuf.*, 2020, **61**, 101848.
7 H. Trung Thien, P. Phuoc Thien, T. Mai Thanh, N. H. Lovell and D. Thanh Nho, *Adv. Mater. Technol.*, 2020, **5**, 2000724.
8 T. Ranzani, G. Gerboni, M. Cianchetti and A. Menciassi, *Bioinspiration Biomimetics*, 2015, **10**, 035008.
9 W.-B. Li, W.-M. Zhang, H.-X. Zou, Z.-K. Peng and G. Meng, *Soft Robot.*, 2019, **6**, 631–643.
10 W. Dou, G. Zhong, J. Cao, Z. Shi, B. Peng and L. Jiang, *Adv. Mater. Technol.*, 2021, **6**, 2100018.
11 B. Tondu and P. Lopez, *IEEE Control Syst. Mag.*, 2000, **20**, 15–38.
12 E. Brown, N. Rodenberg, J. Amend, A. Mozeika, E. Steltz, M. R. Zakin, H. Lipson and H. M. Jaeger, *Proc. Natl. Acad. Sci. U. S. A.*, 2010, **107**, 18809–18814.
13 I. M. Van Meerbeek, B. C. Mac Murray, J. W. Kim, S. S. Robinson, P. X. Zou, M. N. Silberstein and R. F. Shepherd, *Adv. Mater.*, 2016, **28**, 2801–2806.
14 A. Firouzeh, M. Salerno and J. Paik, *IEEE Trans. Robot.*, 2017, **33**, 765–777.
15 T. P. Chenal, J. C. Case, J. Paik and R. K. Kramer, Presented at IEEE/RSJ International Conference on Intelligent Robots and Systems, Chicago, September, 2014.
16 C. Majidi and R. J. Wood, *Appl. Phys. Lett.*, 2010, **97**, 164104.
17 Z. Zhao, S. Zhu, B. Li, C. Niu, Y. Tong, N. Ma, X. Dong, B. Han, H. Huang and M. Qi, *ACS Appl. Polym. Mater.*, 2022, **4**, 2656–2663.
18 P. Jiang, Y. Yang, M. Z. Q. Chen and Y. Chen, *Bioinspiration Biomimetics*, 2019, **14**, 036009.
19 M. A. Robertson and J. Paik, *Sci. Rob.*, 2017, **2**, eaan6357.
20 Y. Wang, L. Li, D. Hofmann, J. E. Andrade and C. Daraio, *Nature*, 2021, **596**, 238–243.
21 D. S. Shah, E. J. Yang, M. C. Yuen, E. C. Huang and R. Kramer-Bottiglio, *Adv. Funct. Mater.*, 2021, **31**, 2006915.
22 M. Cianchetti, T. Ranzani, G. Gerboni, I. De Falco, C. Laschi and A. Menciassi, Presented at IEEE/RSJ International Conference on Intelligent Robots and Systems, Tokyo, November, 2013.
23 M. Manti, V. Cacucciolo and M. Cianchetti, *IEEE Robot. Autom. Mag.*, 2016, **23**, 93–106.
24 T. Hao, *Adv. Mater.*, 2001, **13**, 1847–1857.
25 W. Wen, X. Huang and P. Sheng, *Soft Matter*, 2008, **4**, 200–210.
26 T. Aoyama and I. Inasaki, *CIRP Ann.*, 1997, **46**, 309–312.
27 A. Khanicheh, D. Mintzopoulos, B. Weinberg, A. A. Tzika and C. Mavroidis, *IEEE/ASME Trans. Mechatron.*, 2008, **13**, 286–294.
28 V. A. Bilyk and E. V. Korobko, *J. Intell. Mater. Syst. Struct.*, 2015, **26**, 1906–1912.
29 C. A. Papadopoulos, *Mechatronics*, 1998, **8**, 719–726.
30 J. Madeja, Z. Kesy and A. Kesy, *Smart Mater. Struct.*, 2011, **20**, 105005.
31 A. Mazursky, J.-H. Koo and T.-H. Yang, *J. Intell. Mater. Syst. Struct.*, 2019, **30**, 2521–2533.
32 P. M. Taylor, D. M. Pollet, A. Hosseini-Sianaki and C. J. Varley, *Displays*, 1998, **18**, 135–141.
33 K. Krivenkov, S. Ulrich and R. Bruns, *J. Intell. Mater. Syst. Struct.*, 2012, **23**, 1323–1330.
34 X. Z. Niu, W. J. Wen and Y. K. Lee, *Appl. Phys. Lett.*, 2005, **87**, 243501.
35 Q. A. Nguyen, S. J. Jorgensen, J. Ho and L. Sentis, *Actuators*, 2015, **4**, 135–155.
36 M. Wang and R. Y. Fei, *Smart Mater. Struct.*, 1999, **8**, 511–514.
37 Z. Yuan, L. Wu, X. Xu and R. Chen, *Cognit. Comput. Syst.*, 2021, **3**, 70–77.
38 S. B. Behbahani and X. Tan, *Smart Mater. Struct.*, 2017, **26**, 085014.
39 C. Tang, B. Du, S. Jiang, Q. Shao, X. Dong, X. J. Liu and H. Zhao, *Sci. Rob.*, 2022, **7**, eabm8597.
40 K. D. Weiss, J. D. Carlson and D. A. Nixon, *J. Intell. Mater. Syst. Struct.*, 1994, **5**, 772–775.
41 N. M. Wereley, A. Chaudhuri and J. H. Yoo, *et al.*, *J. Intell. Mater. Syst. Struct.*, 2006, **17**, 393–401.
42 X. Yuan, X. Zhou, Y. Liang, L. Wang, R. Chen, M. Zhang, H. Pu, S. Xuan, J. Wu and W. Wen, *Composites, Part B*, 2020, **193**, 107988.
43 J. R. Amend, Jr., E. Brown, N. Rodenberg, H. M. Jaeger and H. Lipson, *IEEE Trans. Robot.*, 2012, **28**, 341–350.